Repeat Pass Aircraft Interferometery Results at Portage Lake, Maine and Innisfail, Australia

Scott Hensley, Jeff Klein*, Paul Rosen, } laine Chapin, Søren Madsen and Frank Webb

Jet Propulsion Laboratory
4800 Oak Grove Dr
Pasadena, CA 91109

*Rockwel I International

JPL Airborne Earth Science Workshop

Abstract

The NASA/JPL AIRSAR/TOPSAR instruments have the capability of collecting fully polarimetric radar data at three wave.lengths (C, L and P-Bands) and dual antenna interferometry at C-Band, and more recently L-Band. in order to understand frequency and baseline dependent scattering effects in vegetated regions repeat pass interferometry data was collected for two vegetated regions in 1993. Portage Lake, Maine is a primarily coniferous forested region with some clear cutting from logging activities in the region. The second site at Innisfail, Australia borders a tropical rain forest and is situated adjacent to some major clear cut regions and banana plantations. Preliminary analysis of repeat pass data collected in these areas show that the smaller the wavelength the greater the temporal decorrelation between passes, the longer the wavelength the greater the penetration depth for some types of vegetation canopy, yet for some vegetation canopy types, in particular for a banana plantation there appears to be no frequency dependent penetration into the canopy.

Keywords: SAR, interferometry, repeat-pass, vegetation

Introduction

Using two complex SAR images acquired from two spatially separated antennas collected simultaneously, single pass interferometry (SPI), or at different times, repeat pass interferometry (RPI), can be processed to yield elevation maps. The NASA/JPL C-band TOPSAR sensor is one example of an S1'1 interferometer [Zebker et al, 1992]. It is one component of the quadpolarization, three frequency airborne SAR (AI RSAR) operated by JPL. The processing of TOPSAR data into elevation maps is discussed in [Madsen et al, 1993].

It is well known that low frequency radars penetrate foliage better than at high frequencies, thus one might expect that interferometric measurements made at lower frequencies would yield height maps closer to the true ground surface. Until recently no multi-frequency SPI interferometric systems were available (TOPSAR has an L-Band interferometer added in 1995), hence this problem could only be addressed using RPI measurements. Moreover, to get interferometric measurements at wavelengths longer than I.-band requires the usc of RPI data. RPI can be used to generate height maps if 1) the passes arc acquired sufficiently close in time to avoid temporal decorrelation, 2) the baseline vector, vector between the two antenna positions, is shorter than the critical baseline length, and 3) the baseline vector between the two passes is sufficiently constant.

Using repeat-pass interferometry data collected from the AIRSAR multi-frequency, multi-polarimetric radar provides a unique data set for studying frequency and polarization dependent phenomena on interferometric measurements in vegetated regions. Repeat pass data was collected near Portage Lake, Maine, a primarily coniferous forested area, and near Innisfail, Australia, a tropical forested area in Queensland. The radar operating parameters for the TOPSAR C-band mode, and the AIRSAR 1. and P-band polarimetric modes are given in Table 1.

Table 1. Al RSAR/TOPSAR System Parameters

Parameter	C	L	P
Wavelength (m)	.0566	.2422	.6972
Power (w)	1000	5000	1000
Bandwidth (MHz)	40	40	40
Pulse Spacing (m)	.2572	.5144	.5144
Antenna Length (m)	1.5	1.5	1.5
Baseline (m)	2.51		-
Altitude (m)	8100	8100	8100
look Angle (°)	20-60	20-60	20-60
Range (km)	8.5-17	8.5-17	8.5-17
Ground Swath (km)	12	12	12

in order to process RPI data accurate platform position at each pulse event is crucial to determining the interferometric baseline as a function of time [Gray /Farris-Manning 1993]. The NASA/JPL DC-8 is equipped Litton INU (subsequently upgraded to a Honeywell 11764-G integrated GPS/INU), a Turborogue differential GPS receiver, and pulse time tags derived from the GOES satellite. The INU data has an update rate of 50 Hz gives accurate relative position measurements but tends to drift with time. The differential GPS is updated at a 1 Hz rate with estimated position accuracy of 10 cm. Precise platform position information is obtained by combining the INU data with the differential GPS data. These data are linked to the pulse data using the GOES time tag.

Experiment Description

Two sites were selected for study in 1993 using repeat-pass interferometry, onc near Portage Lake in northern Maine and other near Innisfail in Queensland, Australia. The first site has gently rolling terrain with elevations varying between 200 m and 300 m. The area is covered primarily with coniferous forest much of which is second growth due to widespread logging in the region. Vegetation heights vary from a 1 m to 20 m depending on the age and type of vegetation. There arc many clear cut areas in varying stages of regrowth as well as open fields used for agriculture, mostly hay as the land is not particularly well suited for commercial farming.

Considerable ground truth is available for this site since. it has been used extensively by MIT Lincoln 1.aboratory for radar foliage penetration experiments in recent years. Measurements include tree height, canopy structure, biomass and dielectric for selected sites within a 20 km^2 area. in addition four 8 foot trihedral reflectors were deployed in open areas and surveyed using Turborogue GPS receivers as shown in Figure 1 to be used a fiducial points in the images.

The NASA/JPL AIRSAR DC-8 flew eight passes over this site on June. 24, 1993. Each pass was flown attempting to fly the same path each time in the hopes that at least

one pair of passes would be suitable. for RPI processing. As the onboard INU did not measure position and velocity accurately enough for RPI processing differential GPS measurements were acquired using a Turborogue GPS receiver on the plane in conjunction with a reference receiver located near the site (and at the same location used as reference to survey the corner reflectors). Data was collected in the TOPSAR mode at C-band in the AIRSAR 40 Ml Iz quadpolarization mode at I , and P-bands.

The second site is located in Queensland, Australia is situated along the boundary between a tropical rain forest and a clear cut region with cultivation of some crops such a bananas. The topography varies from relatively flat in open areas to very rugged in the tropical forest. The tropical canopy reaches heights of 30 m to 40 m with occasional clearings due to logging.

Ground truth consists of 4 surveyed 8 foot trihedral reflectors deployed in open areas adjacent to the rain forest. In addition to the corner reflectors used as fiducial points, canopy measurements including tree heights and canopy structure were obtained by MIT Lincoln Laboratory.

The NASA/JPL AIRSAR DC-8 flew eight passes over this site on September 4, 1993. As described previously each pass was flown attempting to fly the same path each time in the hopes that at least one pair of passes would be suitable for RPI processing. Also as before Turborogue differential GPS measurements were acquired using a Turborogue GPS receiver on the plane in conjunction with a reference receiver located near the site (and at the same location used as reference to survey the corner reflectors). Data was collected in the TOPSAR mode at C-band in the AIRSAR 40 MHz quadpolarization mode at L and P-bands.

Data Processing

Processing of the RPI data consists of four major steps, 1) the Turborogue differential GPS measurements arc combined with the INU data to obtain accurate platform position vectors, 2) the RPI passes over a given site arc analyzed to determine which ones (if any) arc suitable for interferometric processing 3) the data arc converted to an appropriate coordinate system and processed into interferograms 4) residual motion measurements arc made directly from the data and the scene processed to a height map.

Turbor ogue data collected onboard the aircraft is processed at JPL using J1'L derived ephemeris vectors for GPS satellites, models for ionospheric and tropospheric delays, yielding position vectors with an estimated accuracy of 10 cm [Webb et al, 1993]. These data arc then combined with the INU data by high pass filtering the INU data and combining it with GPS data using a least squares approach as described in [Madsen et al, 1993].

Next pairs of repeat pass lines arc examined to find suitable pairs for RP1 processing. One pass is arbitrarily chosen as reference and the platform position vectors arc converted into a convenient coordinate frame, the "(s,c,h)" coordinate system where s, c and h arc respectively the along track, cross track, and altitude coordinates of a "best fit" spherical approximation to the ellipsoid centered at the middle of the track. The (s,c,h) coordinate frame is not a Cartesian frame, but a spherical coordinate system designed to locally approximate the WGS-84 ellipsoid. 'l'his reference sphere is chosen to bc locally tangent to the ellipsoid at a reference point called the peg point, and to have radius equal to the radius of curvature in the along track direction as shown in Figure 1.

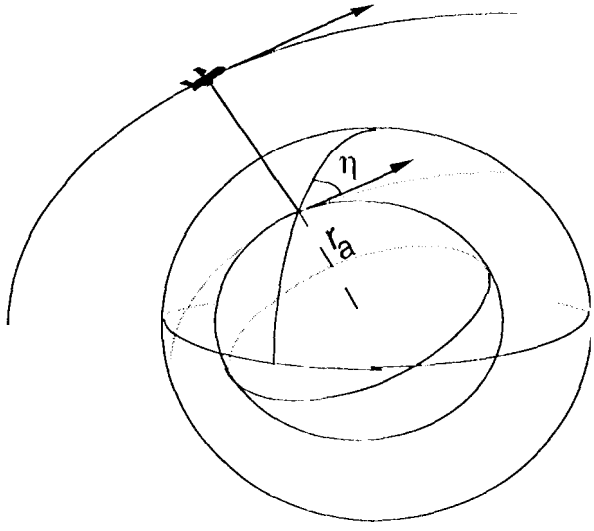

Figure 1. Approximating sphere used to define the (s,c,h) coordinate system.

in the (s,c,h) system s denotes the distance along the reference curve from the peg point, which is a great circle in the approximating, sphere, c is the distance along the arc perpendicular to the reference curve, and h is the height above the reference sphere,

The transformation from radar mapping coordinates, (s,c,h), to WGS-84 coordinates, (x,y,z). The radar mapping coordinates are defined relative to the. sphere. tangent to the ellipsoid at $(\theta 0,\lambda 0)$, having radius r_a which is the radius of curvature in the along track direction given by

$$r_a = - \frac{r_e(\lambda_0)\ r_n(\lambda_0)}{r_e(\lambda_0)\cos^2(\eta) - t\ r_n(\lambda_0)\ \sin^2(\eta)}$$

where η is the heading (actually track angle) and r_e and r_n arc the radii of curavature in the cast and north directions respectively given by

$$r_e(\lambda) = - \frac{a}{\left(1 - e^2\ \sin^2(\lambda)\right)^{\frac{1}{2}}} \qquad r_n(\lambda) = - \frac{a\,(1 - e^*)}{(1 - e?\ \sin^2(\lambda))^{\frac{3}{2}}}$$

The point $(\theta 0,\lambda 0)$ will be referred to as the peg point and the sphere as the approximating sphere. Take the equator of the approximating sphere to be the reference curve (i.e. reference track), assumed to be a great circle on the approximating sphere. The prime meridian to the approximating sphere is the intersection of the approximating sphere and the plane determined by the unit normal vector, U, to the ellipsoid and the cross track vector C = U x T where T is the unit tangent vector to the. reference curve. The radar mapping coordinates (s,c,h) are defined as the distance along the reference curve from the peg point, the distance from the reference curve along a meridian at a distance s from the peg point, and the height above the approximating sphere respectively. Let (x´,y´,z´) be geocentric coordinates for the approximating sphere where the x‘ axis is U, the y’ axis is T and the z´ axis is C. Then the transformation from mapping coordinates to x’y´z´ coordinates is

$$\begin{pmatrix} x' \\ y' \\ z' \end{pmatrix} \equiv \begin{pmatrix} (r, -t\,h)\cos(c_\lambda)\cos(s_\theta) \\ (r, +\,h)\cos(c_\lambda)\sin(s_\theta) \\ (r_a + h)\sin(c_\lambda) \end{pmatrix}$$

where $c_\lambda = c/r_a$ and $s_\theta = s/r_a$. The transformation from $x'y'z'$ to xyz coordinates is an affine transformation of the form

$$\begin{pmatrix} x \\ y \\ z \end{pmatrix} = M^{xyz}_{ENU}\, M^{ENU}_{x'y'z'} \begin{vmatrix} x' \\ Y' \\ z' \end{vmatrix} + o$$

where O is a translation vector, M^c_b is the transformation matrix from frame b to frame c, and the ENU frame is a basis for the tangent space at the. peg point with E a unit vector in the east direction and N a unit vector in the north direction. To obtain the transformation matrix from x 'y 'z' to ENU observe that t hey arc related by a rotation about the U (or x') axis by the track angle η. Thus the $x'y'z'$ to ENU transformation matrix is

$$M^{ENU}_{x'y'z'} \cdot \begin{vmatrix} 0 & \sin(\eta) & -\cos(\eta) \\ o & \cos(\eta) & \sin(n) \\ 1 & 0 & 0 \end{vmatrix}.$$

The transformation matrix from ENU to xyz is just the matrix formed by the column vectors of E,N, and U in xyz coordinates. The transformation matrix is

$$M^{xyz}_{ENU} = \begin{vmatrix} -\sin(\theta_0) & -\sin(\lambda_0)\cos(\theta_0) & \cos(\lambda_0)\cos(\theta_0) \\ \cos(\theta_0) & -\sin(\lambda_0)\sin(\theta_0) & \cos(\lambda_0)\sin(\theta_0) \\ 0 & \cos(\lambda_0) & \sin(\lambda_0) \end{vmatrix}$$

The translation vector O is given by

$$O = P - r_a U$$

where $P=(r_e(\lambda_0)\cos(\lambda_0)\cos(\theta_0), r_e(\lambda_0)\cos(\lambda_0)\sin(\theta_0), r_e(\lambda_0)(1-e^2)\sin(\lambda_0))$ is the vector from the center of the ellipsoid to the peg point.

After conversion of the platform position vectors to (s,c,h) coordinates of the reference path, the data aligned in time to compute the instanteous baseline vector, The instantaneous baseline vectors is computed as follows. For each point on the reference track the instantaneous imaging plane is computed from the yaw and pitch angles. The intersection of this plane with the second track gives onc candidate baseline vector. A second candidate results from taking the imaging plane from the point and finding its intersection on the first track. Finally, the intersection of the imaging plane at this point wit h t he second track is computed. The reference track is given by the average of these four vectors and the normal to the imaging plane determined by the average of the normals to the four imaging planes. This is illustrated in Figure 2. The instantaneous baseline is difference the intersections of the imaging plane from a point on the reference track to the two tracks. Baselines for each pair of passes are examined for length and convergence rates. Track with length from 15-50 meters and small convergence rates are the most desired.

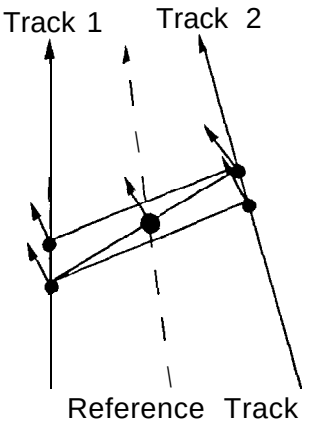

Figure 2. Determining the reference path and instantaneous baseline.

After selection of an appropriate RPI pair the data are motioned compensated first to dual references tracks and then to a single reference track as described in [Stevens et al, March 1995]. Using the single reference track approach the offsets between the two single look complex (SLC) images used to form the interferogram should be zero. Height reconstruction uses a modified form of the height reconstruction equations outlined in [Madsen et al, 1993].

Results

At Portage Lake, Maine one pair of passes taken 30 minutes apart was suitable for RPI processing and the baseline as a function of along track position is shown in Figure 3. Amplitude images of all three passes are shown in Figure 4. Note that the flat open areas have progressively less backscatter as the wavelength increases whereas in the vegetated regions all three frequencies are relatively bright, Figure 5 shows C, 1, and P-band RPI inteferograms. One cycle of color corresponds to 2π radians of phase. The flat earth fringes are removed during the motion compensation process except for fringes due to topography and residual baseline errors. Figure 6 shows the TOPSAR generated topographic map. Note (he close agreement of the P-band fringes with the TOPSAR height map. The higher azimuth fringing visible in both the C and I.-band interferograms is a result of residual baseline errors. The magnitude of residual baseline can be est i mat ed from the along track offsets bet wcen the two single look complex images used to form the interferogram. These offsets would be zero if knowledge of the baseline was perfect. A plot of the azimuth offsets as a function of along track position for five ranges is shown in Figure 7. Using a simple sinusoidal model for cross track position error as a function of along track position shows that the magnitude of the residual baseline error is approximatel y 6 cm. A subsequent paper will discuss estimat ion of these errors from the data.

A comparison of the interferometric correlation for the three frequencies is quite interesting and is shown in Figure, 8. In this figure blue denotes a correlation of ,25 or below and yellow a correlation 1.0. Note the almost complete decorrelation of the C-band interferogram in the vegetated areas while the clear cut areas are highly correlated, This can be compared with the TOPSAR correlation map shown in Figure 6 where the correlation is generally above .9 in all areas. There is a dramatic increase in correlation in the vegetated regions for L and P-bands, however correlation in the fl at open areas is quite poor particularly at P-band as a result of the low backscatter. Wc conclude that the

dramatic drop in decorrelation as wavelength decreases is due to temporal decorrelation. Small motions in the leaves and branches on the order of one tenth a wavelength cause the C-band to decorrelate faster than either L or P-bands.

Because of the relatively short baseline of 15 m, the fringe frequency is quite small and unwrapping the P-band data is not too difficult, however because the baseline is almost completely horizontal the ambiguity height (height change for one cycle of phase) varies from 60 m in the near range to 600 m in the far range. The greatly reduces the height acuity in the far range. Figure 9 shows a P-band RPI height map. The height accuracy varies from 3-30 m from near to far range making height comparisons with the TOPSAR DEM useless in the far range.

For the Innisfail, Australia data one pass was found to be suitable for RPI processing, however the baseline in this case is approximately 100 m. Figure 10 shows the TOPSAR generated DEM and L and P-band RPI interferograms. The TOPSAR DEM is shown in the upper left corner with one cycle of color equal to 150 mete.rs, the ambiguity height at L-band. No attempt was made to remove residual baseline errors from the interferograms, hence there are slight ramps in both range and azimuth. The bright region in the upper left portion of the TOPSAR DEM is a banana plantation. Figure 11a shows a cut through the trees, from which a tree height of approximate] y 7-8 meters is inferred. After removing a t i lt from the unwrapped P-band interferogram a cut through the banana plantation is shown in Figure 11b. Using an ambiguity height of 50 m for P-band the phase difference corresponds to roughly 8 m in good agreement with the C-band data. Figure BBB shows the difference between the 1. and P band interferograms where the P -band phase has been scaled by the ratio of the wavelengths to match the L-band fringe, rate. A cut through the phase difference plot is shown in Figure 11 c. The phase difference corresponds to less than a meter. This indicates there is no differential penetrat ion as a function of wavelength for the banana grove.

Conclusions

Preliminary analysis of repeat pass data collected in these areas show that the smaller the wavelength the greater the temporal decorrelation between passes, the longer the wavelength the greater the penetration depth for some types of vegetation canopy, yet for some vegetation canopy types, in particular for a banana plantation there appears to be no frequency dependent penetration into the canopy for the three. frequencies.

Acknowledgments

Wc would like to thank M. Moghaddam and D. Haub for their participation in this experiment, JPL Aircraft Radar Group for collecting this data, and MIT Lincoln laboratory (particularly R. Downing) for valuable assistance in setting up the experiment.

References

[1] Zebker, H.A. et al, "The Topographic Interferometric Radar Mapping instrument", *IEEE Trans on Geoscienc and Remote Sensing,* V30, No. S, Sept. 1992.

[2] Madsen, S. N., Zebker, H. A., Martin, J., '(Topographic Mapping Using Radar Interferometry: Processing Techniques", *IEEE Trans* on *Geoscienc and Remote Sensing*, V.31, No. 1, Jan. 1993.

[3] Gray, A.L. and Farris-Manning, P, J., "Repeat Pass Interferometry with Airborne Synthetic Aperture Radar", *IEEE Trans on Geoscienc and Remote Sensing*, V.31, No.1, Jan. 1993.

[4] Webb, 1:.11. and Zumberge, J. F. (editors), *An Introduction to GIPSY/OASIS-II*, JP1, Document D-1 1088, July 1993.

[5] Stevens, D. R., Cumming, I. G., and Gray, A. L., " options for Airborne Interferometric SAR Motion Compensation", *IEEE Trans on Geoscience and Remote* Sensing, V.33, No. 2, Mar. 1995.

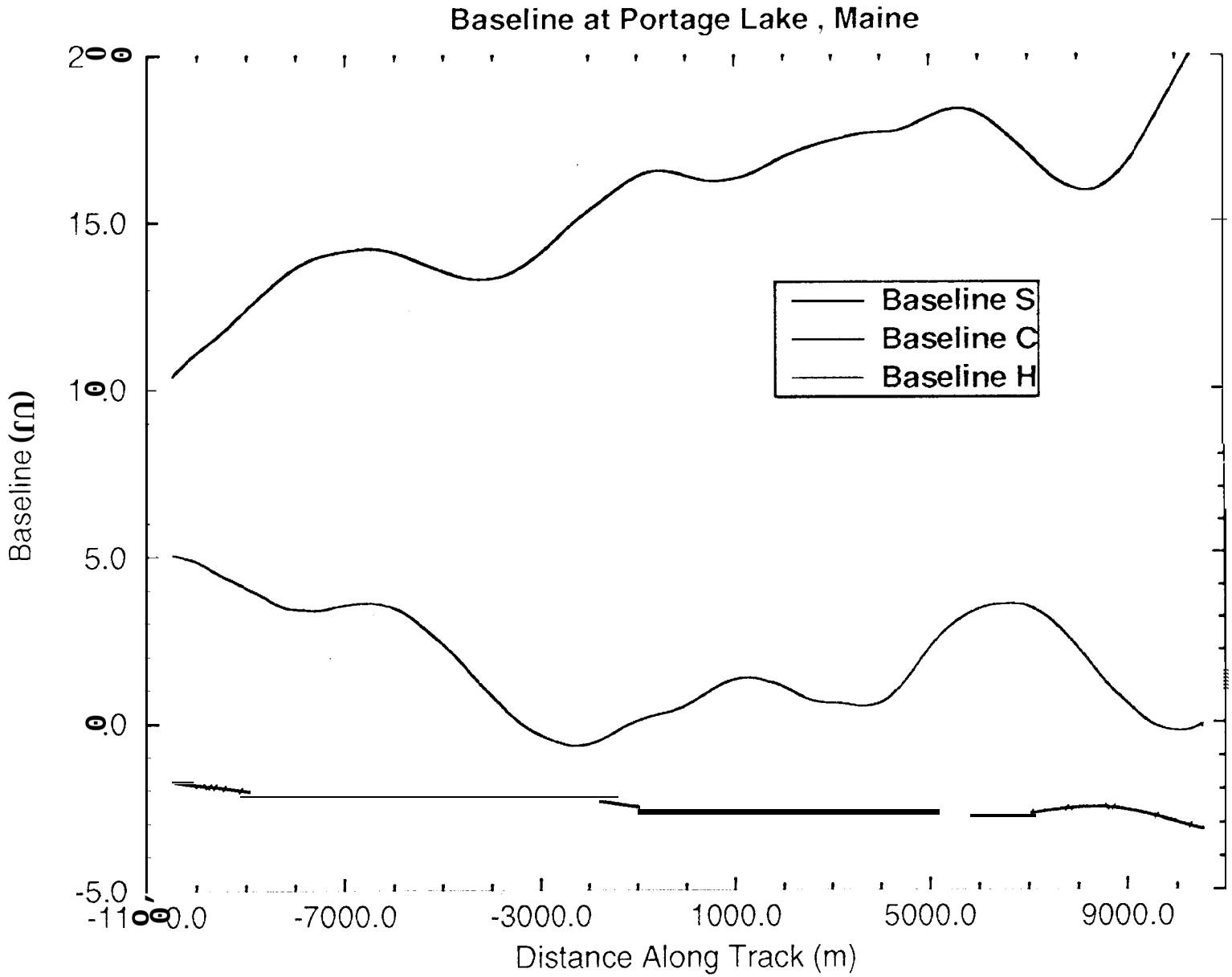
Baseline at Portage Lake , Maine
Baseline S
Baseline C
Baseline H
Baseline (m)
15.0
5.0
-5.0
-7000.0
-3000.0
1000.0
5000.0
9000.0
Distance Along Track (m)

Figure 3.

JPL

Multi-Frequency Aircraft Interferometry

Amplitude Imagery

C L P

Figure 4.

JPL

Multi-Frequency Aircraft nterferometry

Interferograms

C-band Repeat

L-band Repeat

P-band Repea

Figure 5.

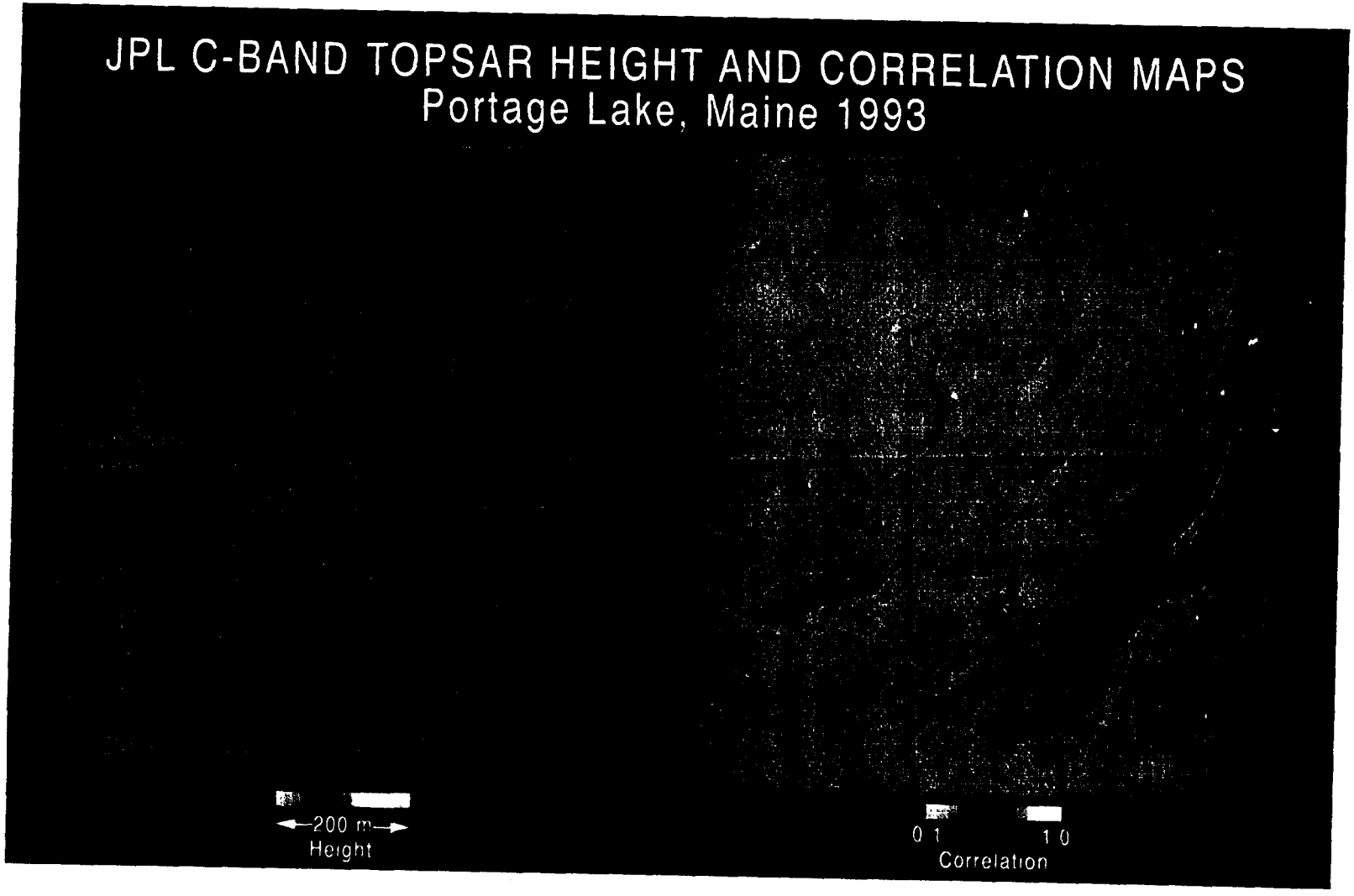
JPL C-BAND TOPSAR HEIGHT AND CORRELATION MAPS
Portage Lake, Maine 1993
200 m
Height
0 1
1 0
Correlation

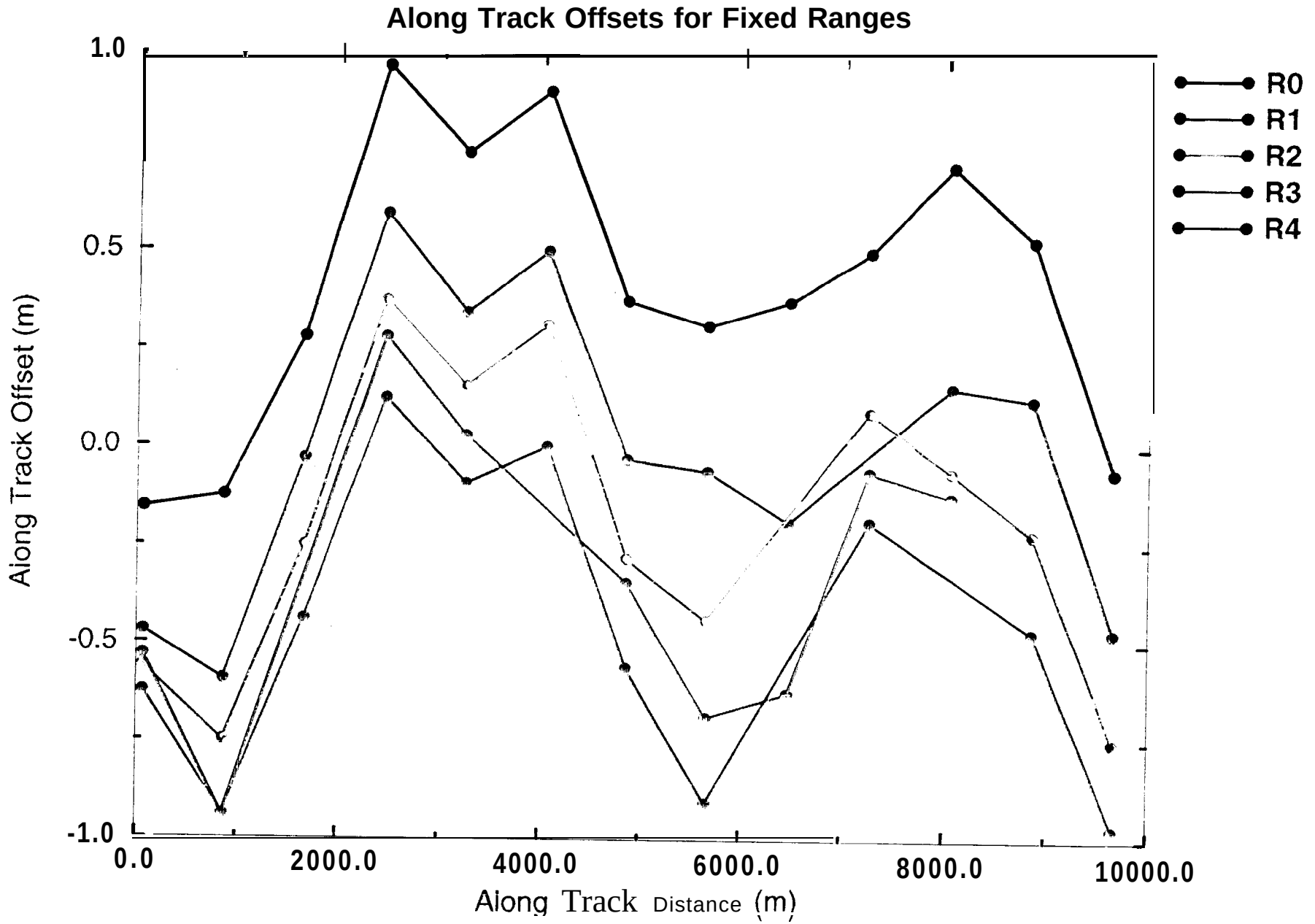
Along Track Offsets for Fixed Ranges
1.0
0.5
0.0
-0.5
-1.0
Along Track Offset (m)
0.0
2000.0
4000.0
6000.0
8000.0
10000.0
Along Track Distance (m)
R0
R1
R2
R3
R4

JPL

Multi-Frequency Aircraft Interferometry

Correlation Maps

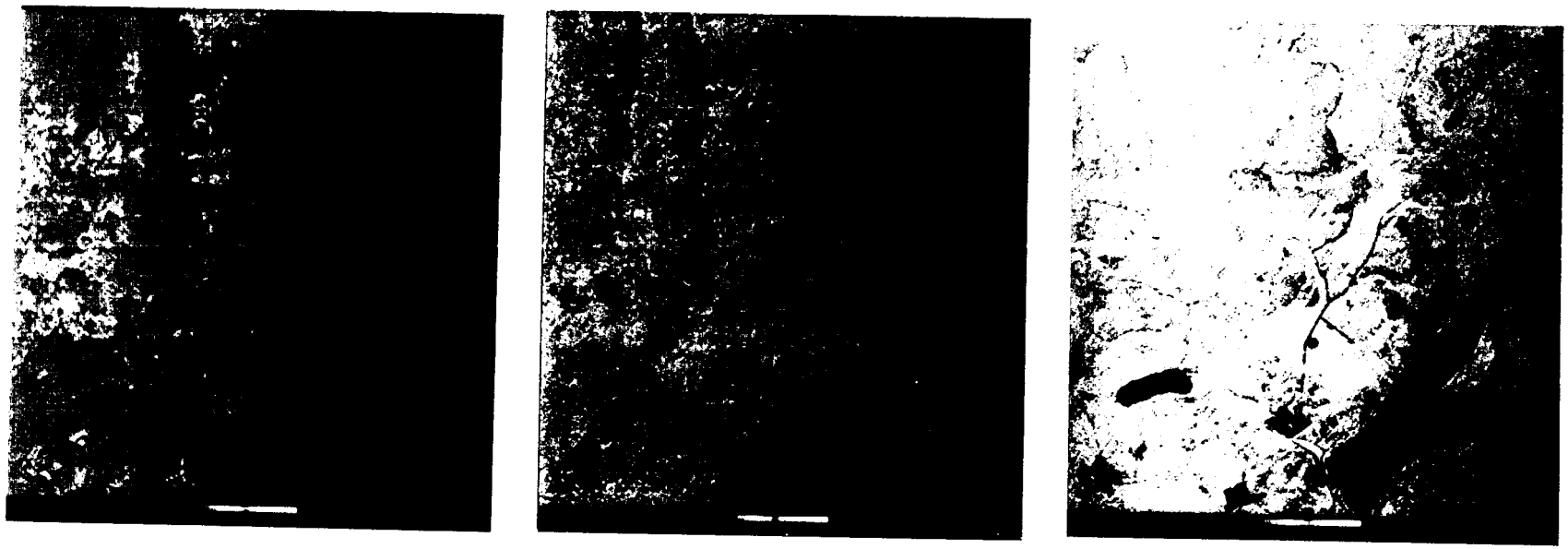

C-band Repeat **L-band Repeat** **P-band Repeat**

Figure 8.

Figure 9.

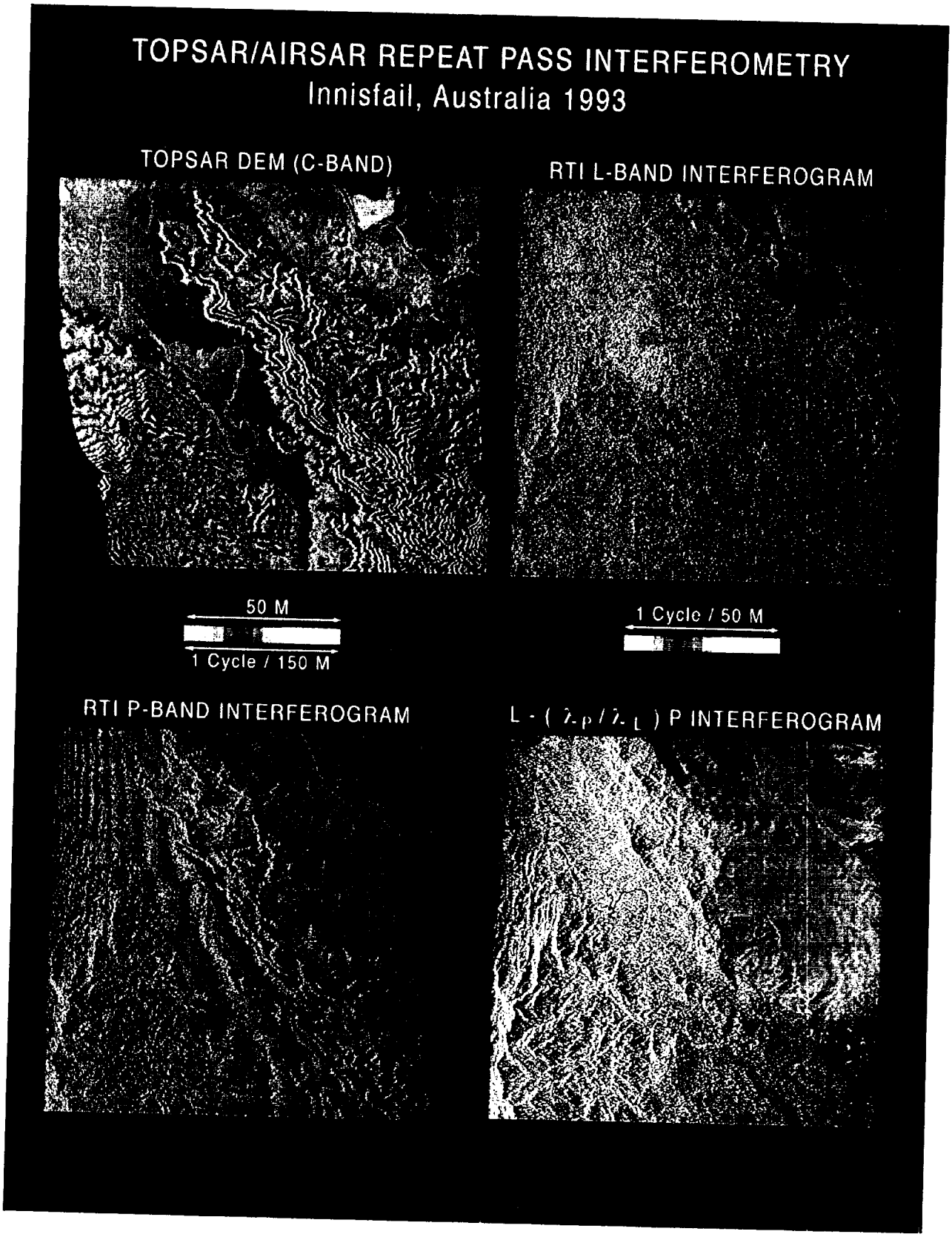
TOPSAR/AIRSAR REPEAT PASS INTERFEROMETRY
Innisfail, Australia 1993
TOPSAR DEM (C-BAND)
RTI L-BAND INTERFEROGRAM
50 M
1 Cycle / 150 M
1 Cycle / 50 M
RTI P-BAND INTERFEROGRAM
L - (λP / λL) P INTERFEROGRAM

Figure 10.

Innisfail, Australia C-Band Topsar Heights

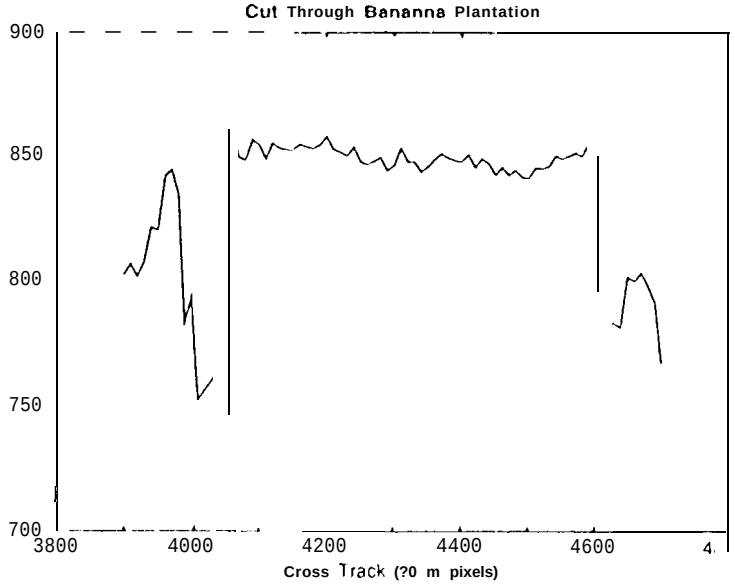

Cut Through F'-Band Aircraft Interferogram

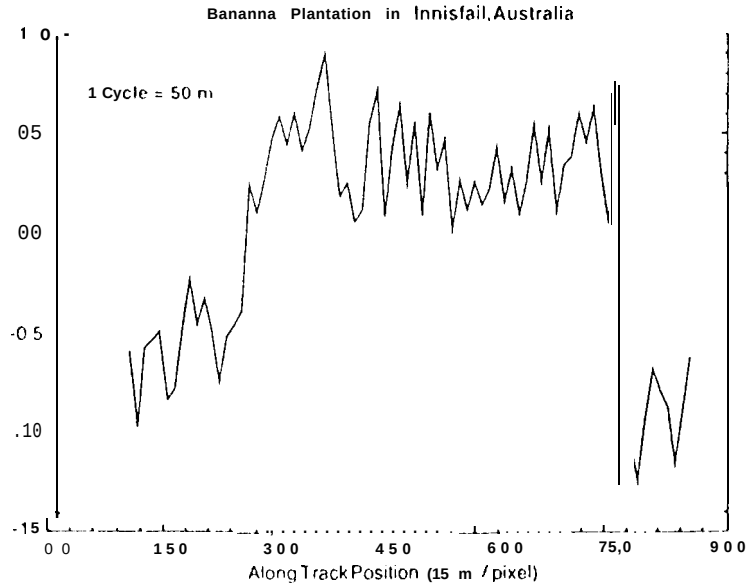

Innisfail, Australia L-P Difference

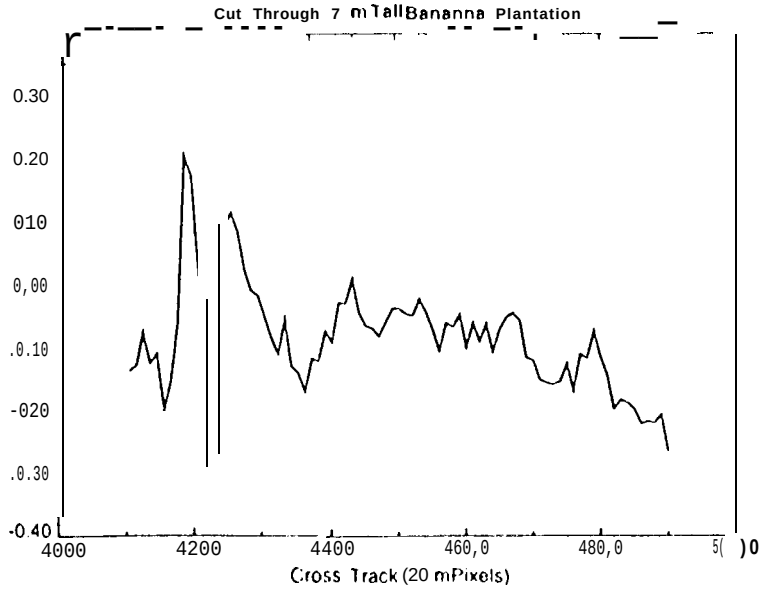

Figure 11.